IEEE Photonics Journal
An IEEE Photonics Society Publication

Open Access

# Efficient TE-Polarized Mode-Order Converter Based on High-Index-Contrast Polygonal Slot in a Silicon-on-Insulator Waveguide

Volume 11, Number 2, April 2019

Lijun Hao
Rulei Xiao
Yuechun Shi
Pan Dai
Yong Zhao
Shengping Liu
Jun Lu
Xiangfei Chen

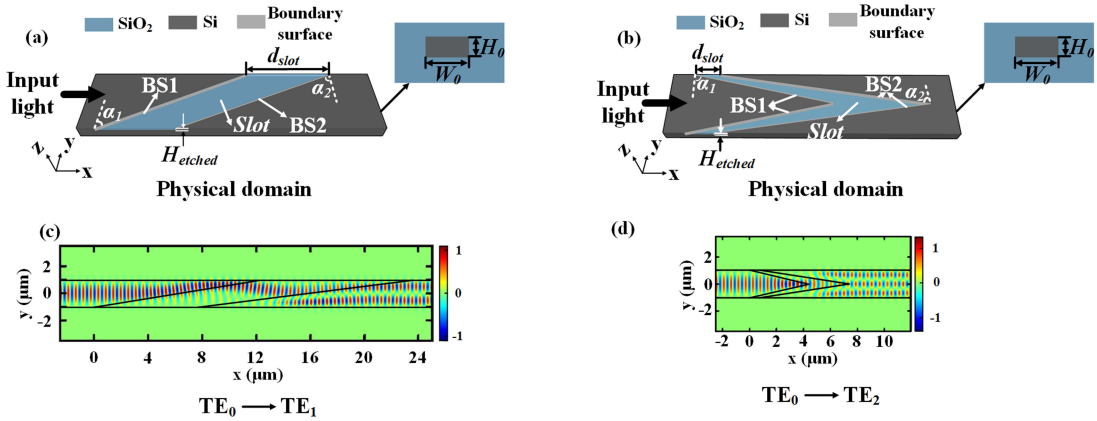


DOI: 10.1109/JPHOT.2019.2907640
1943-0655 © 2019 IEEE

# Efficient TE-Polarized Mode-Order Converter Based on High-Index-Contrast Polygonal Slot in a Silicon-on-Insulator Waveguide

**Lijun Hao, Rulei Xiao, Yuechun Shi, Pan Dai, Yong Zhao, Shengping Liu, Jun Lu, and Xiangfei Chen**

Key Laboratory of Intelligent Optical Sensing and Manipulation of the Ministry of Education, and National Laboratory of Solid State Microstructures, and College of Engineering and Applied Sciences & Institute of Optical Communication Engineering, Nanjing University, Nanjing 210093, Jiangsu China

*DOI:10.1109/JPHOT.2019.2907640*


Manuscript received March 5, 2019; revised March 21, 2019; accepted March 23, 2019. Date of publication March 26, 2019; date of current version April 17, 2019. This work was supported by the Chinese National Key Basic Research Special Fund under Grant 2017YFA0206401; Jiangsu Science and Technology Project under Grant BE2017003-2; National Natural Science Foundation of China under Grants 61435014, 11574141, 61504170, and 61504058; Natural Science Foundation of Jiangsu Province under Grant BK20160907; Fundamental Research Funds for the Central Universities under Grant 021314380113. Corresponding author: Yuechun Shi (e-mail: shychnj@163.com).

**Abstract:** We proposed a new type of transverse electric (TE) polarized mode-order converter based on a deeply-etched polygonal slot on a silicon-on-insulator waveguide. Along the transverse direction of the waveguide, two irregular boundary surfaces of the slot can introduce high-contrast index modulation on guided modes, leading to multimode interference in the slot. Therefore, when the slot is optimized, we can achieve efficient mode conversions based on the multimode interference. As examples, mode converters from the fundamental TE mode ($TE_0$) to the first-order TE mode ($TE_1$) and to the second-order TE mode ($TE_2$) have both been demonstrated with a short device length ($<$24.0 $\mu$m), a high mode conversion efficiency ($>$97.6%), and a low modal crosstalk ($< -20.0$ dB) over a broad wavelength range from 1500 to 1600 nm ($\sim$100 nm). In addition, based on different polygonal slots, other types of mode conversions such as from $TE_1$ to $TE_3$ and from $TE_2$ to $TE_1$ have be realized. Fabrication tolerance of the proposed structure is analyzed. Owing to the high efficiency and compact size, the proposed structure could be applied to on-chip mode division multiplexing systems for high-density integration.

**Index Terms:** Integrated optics devices, mode conversion, silicon photonics.

## 1. Introduction

Photonic integrated circuits (PICs) has attracted great interests owing to the potential in the fields of optical information processing, data communicating and optical sensing [1]–[3]. For PICs, manipulation of guided modes is of great importance since the guided modes can be used as signal carriers in the MDM systems and can further scale the transmission capacity of the optical interconnection [4], [5]. Various optical devices have been proposed to construct the MDM circuits, such as mode multiplexers, mode filters, mode switches, mode converters, and mode splitters [6]–[9]. Among

them, the mode converter is a key component for MDM systems and can also be applied into other integrated photonic devices such as nanofocusing, bio-sensors and optical isolators [10]–[12].

Up to now, various mode converters have been proposed. Three methods are usually utilized for mode conversions: (1) phase matching; (2) beam shaping; and (3) coherent scattering [13]–[16]. Based on these methods, mode conversions that are realized by gradual index change or low-contrast index modulation such as tapers and Bragg gratings, cannot well address the challenges like the large device footprint, limited operation bandwidth and robustness, lack of scalability for more mode order conversion. Recently, some methods based on high-contrast index modulation have been proposed as attractive solutions for solving these problems [17]–[20]. For examples, mode converters based on metasurfaces or photonic crystals can strongly control the phase and magnitude of guided modes. In the metasurfaces based on periodic deeply-etched subwavelength structure, phase matching is satisfied for different order mode conversion [17], [18]. Besides, in the metasurfaces based on silicon nanoantenna arrays on $LiNbO_3$ or $Si_3N_4$ waveguides, coherent scattering between guided modes and gradient phased arrays can also be utilized to convert the mode order [19]. In addition, beam shaping in the deeply-etched trenches has been proposed [21]. Based on high-contrast index modulation, the on-chip manipulation of guided modes is of high efficiency. Therefore, the footprints of these devices are highly reduced with a broadband operation, which will be beneficial for the large-scale high-density integration in PICs.

However, the method of high-contrast index-modulation is limited by the high-index materials in nature [22]. Therefore, we propose a new method to equivalently realize higher index-contrast modulation by designing the geometry of the waveguide through transformation optics (TOs). Since the TOs was first proposed by Leonhardnt and Pentry *et al*. the TOs has been utilized as a new method to obtain desired electromagnetic responses [23], [24]. However, the transformed materials properties are complex, which raises significant challenges to the experimental realization. Therefore, we use the inverse conformal mapping to solve for the material properties and help to analyze optical devices with irregular geometry.

In this paper, we propose a new type of mode converter based on polygonal deeply-etched slot in the silicon waveguide. Due to the irregular geometry of the slot, high-contrast index modulation is introduced by the BSs of the slot, which results in multimode interference in the slot. By optimizing the polygonal slot, efficient mode conversion can be realized. The proposed mode converter from $TE_0$ to $TE_1$ and from $TE_0$ to $TE_2$ both show a high mode conversion efficiency ($>$97.6%), and a low modal crosstalk ($< -20.0$ dB) over a broad wavelength range from 1500 nm to 1600 nm ($\sim$100 nm).

## 2. Principle

Our proposed mode converter is based on multimode interference in the deeply-etched polygonal slot, which can be optimized for efficient mode conversion. Two irregular BSs of the slot can introduce high-contrast index distribution with several high index regions (HIRs) which will act as the selectively-scattering input ports, the light-guiding output ports for multimode interference in the slot. Therefore, when the input mode propagates through the first boundary surface (BS1), the mode will be firstly squeezed into the high index regions (HIRs) on BS1 and then scattered into multiple eigenmodes. Afterwards, the multiple eigenmodes interfere with each other in the slot waveguide. The second boundary surface (BS2) is designed at the position where specific field distribution is formed and guide the light by HIRs along the BS2. Besides, due to the high-contrast index change along the BS2, a $\pi$ phase difference is introduced in the adjacent propagating beams. Thus an efficient mode conversion can be achieved with the optimized slot.

### *2.1 High-Contrast Index Modulation*

The schematic of two TE-polarized mode-order converters based on tilted slot and bi-tilted slot in the physical domain are depicted in Fig. 1(a) and (b) respectively. For both tilted slot and bi-tilted slot, the polygonal slot is deeply etched in the silicon waveguide and filled with silica. In addition, the substrate and the cladding materials are designed to be silica to increase conversion efficiency

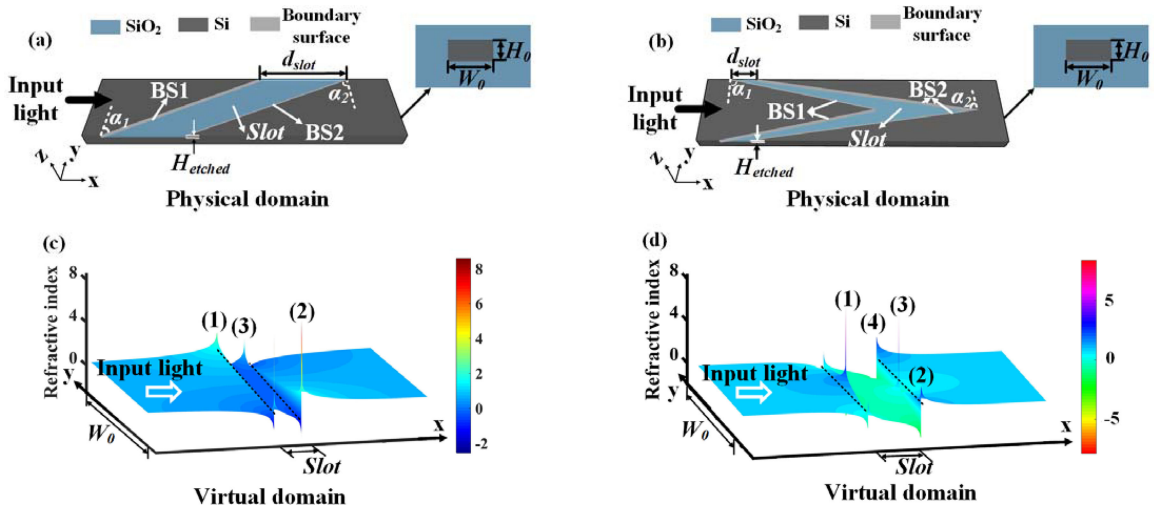


Fig. 1. Schematic of (a) tilted slot and (b) bi-tilted slot deeply-etched in the silicon waveguide in the physical domain. The substrate and the cladding materials are silica which is omitted to clearly show the polygonal slot. The polygonal slot is fulfilled with silica. Refractive index distribution introduced by (c) tilted slot and (d) bi-tilted slot in the virtual domain.

and robustness of our proposed structure. The SOI waveguide width $W_0$ is 2.0 $\mu$m and the height $H_0$ is 220.0 nm. The etched depth of the slot is $H_{etched}$, and the distance between two BSs on the upper sidewall of the waveguide is denoted as $d_{slot}$. Besides, the angle of the two BSs are $\alpha_1$ and $\alpha_2$ respectively. The bi-tilted slot is of an arrow-like shape which shows even symmetry along the transverse direction of the waveguide. The geometry of the proposed polygonal slot can be arbitrary according to the required mode order conversion. Here, tilted slot and bi-tilted slot are taken as two simple examples to analyze mode conversion properties.

Due to the irregular geometry of the polygonal deeply-etched slot, it is hard to analyze the propagation of light along the slot in the physical domain with light being focused at the sharp corners. Therefore, we use the inverse Schwarz-Christoffel (SC) mapping to transform the polygonal slot in the physical domain into a rectangular slot in the virtual domain. The refractive index distribution of the rectangular slot can be calculated according to the mapping relation [23], [25], [26]. Therefore, the polygonal slot in the physical domain can be equivalently analyzed with the index distribution in a mapped rectangular slot in the virtual domain. For the convenience of discussion, our optical transformation is limited to a two-dimensional (2D) plane with transverse electric (TE) field incidence. Fig. 1(c) and (d) show the calculated refractive index distribution introduced by tilted slot and bi-tilted slot in the virtual domain respectively.

It should be noted that in our proposed mode converters, the angles of the two BSs are larger than 70°. Therefore, the corners of the polygonal slot would be extremely sharp and the refractive index gets extremely high (larger than $10^4$) at sharp corners [27]. Therefore, to clearly show the refractive index distribution, we plot the logarithm of the calculated refractive index at the base of 10. In addition, in Fig. 1(c) and (d), the color legend is different for tilted slot and bi-tilted slot because the difference in their refractive index distribution makes it hard to both display the two distributions clearly with the same legend.

By the inverse SC mapping, the two irregular BSs of the polygonal slot in the physical domain can be mapped to the two straight BSs in the virtual domain. For the tilted slot, as shown in Fig. 1(c), high-contrast index distributions are formed along the two virtual BSs with four high index regions (HIRs) of varying extreme values. The HIRs are in accordance with the vertices of the BSs in the physical domain. However, one HIR on the BS1 has little influence on the propagation of the light since light has already been gradually squeezed into port (1). Therefore, we only labeled the other three HIRs as port (1), (2) and (3) respectively. For the bi-tilted slot, high-contrast index distribution

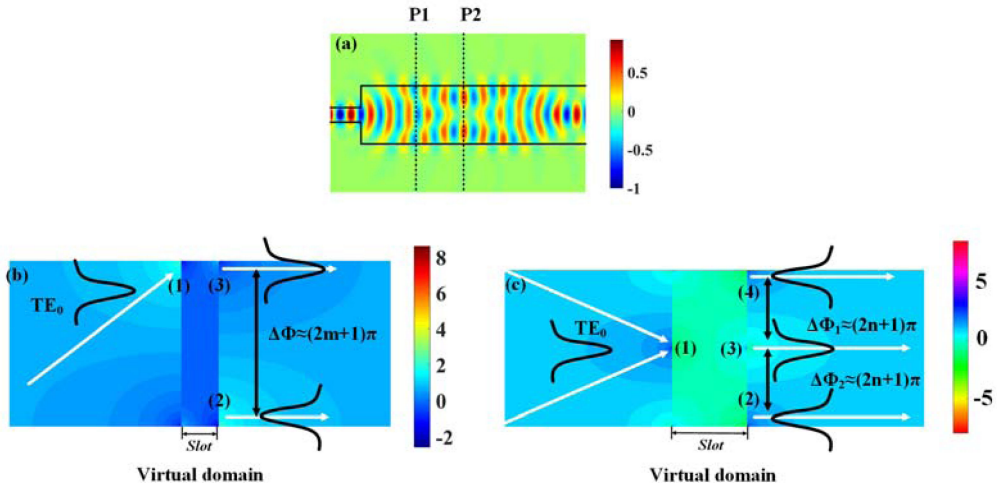


Fig. 2. (a) Electric field ($E_y$) distribution of the general multimode interference with $TE_0$ inputted. Two-dimensional (2D) calculated refractive index distribution introduced by (b) tilted slot and (c) bi-tilted slot together with the mode conversion process, respectively. The white arrow shows the propagation direction of the light.

also formed along the two virtual BSs. Likewise, even though there are six HIRs along the virtual BSs and only four working HIRs are labeled as port (1), (2), (3) and (4). Besides, the positions of the HIRs is also different for the bi-tilted slot and the tilted slot.

### *2.2 Mode Conversion by Multimode Interference*

Since the refractive index in the HIRs along the virtual BSs are extremely high, light can be focused into HIRs. When $TE_0$ is inputted, it can be focused into HIRs on the BS1 and then scattered into multiple eigenmodes in the slot waveguide, leading to multimode interference [28]. However, one difference from general MMI devices as shown in Fig. 2(a) is that the magnitude of scattered eigenmodes can be varied with the change of the angle of the BS1 $\alpha_1$, thus the field distribution of multimode interference is changed accordingly. Therefore, the port (1) in the tilted slot and the bi-tilted slot act as a selectively-scattering input port of the multimode interference. When the field distribution of multimode interference forms two beams of same phase as position 2 (P2) in Fig. 2(a), for tilted slot, the two HIRs on the BS2 can focus the two beams of light into silicon waveguide. In addition, with the high-contrast index change along BS2, the accumulated phase difference between the two beams of light will be $\Delta\Phi \approx (2m + 1)\pi$ where m is an integer. Therefore, mode conversion from $TE_0$ to $TE_1$ is achieved with the slot optimized. Likewise, for bi-tilted slot, BS2 should be designed at position 1 (P1) as shown in Fig. 2(a) and light would be guided by port (2), (3) and (4) with the adjacent phase difference also being $\Delta\Phi_1 \approx (2n + 1)\pi$ and $\Delta\Phi_2 \approx (2n + 1)\pi$, n is an integer. Therefore, the mode conversion from $TE_0$ to $TE_2$ can also be achieved.

In summary, efficient TE-polarized mode order conversion such as from $TE_0$ to $TE_k$ is illustated in Fig. 3. There are three conditions need to be satisfied simultaneously:

1) Field distribution of multimode interference in the slot waveguide should be able to form $(k + 1)$ beams of light. Since the multimode interference is determined by the magnitudes of eigenmodes $\vec{e}_i^{Slot}$ scattered by BS1, the shape of BS1 including the vertices numbers, their positions and interior angles can be determined by examining the scattered field distribution.
2) The $(k + 1)$ beams of the scattered field in the slot can be well-guided by BS2 into the silicon waveguide and each beam has a $\pi$ phase difference with adjacent beams. This process can be achieved by optimizing the shape of BS2.

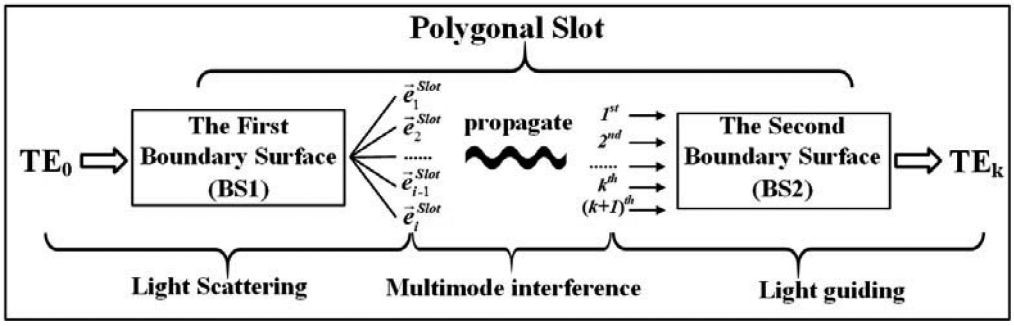


Fig. 3. Schematic of mode conversion from $TE_0$ to $TE_k$.

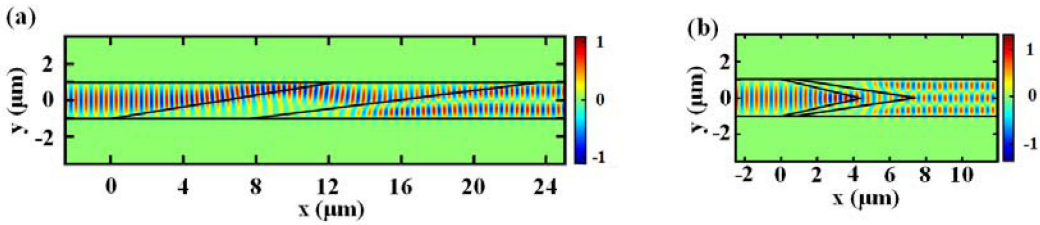


Fig. 4. Electric field ($E_y$) distribution along the mode converter (a) from $TE_0$ to $TE_1$ based on tilted slot and (b) from $TE_0$ to $TE_2$ based on bi-tilted slot.

3) After BS1 and BS2 are determined, the distance between BS1 and BS2 should be adjusted to make (k + 1) beams of the field distribution by multimode interference consistent with the position of BS2.

Therefore, light scattering on BS1, light guiding on BS2 with proper phase difference and the distance between BS1 and BS2 all need to be properly designed with the optimization of structure parameters such as the shape of the BSs, the etched slot depth $H_{etched}$, the angles of the two BSs $\alpha_1$ and $\alpha_2$, and the distance between the BSs $d_{slot}$.

## 3. Simulation Results

Our proposed mode converter is based on high-contrast index modulation introduced by the polygonal slot and can realize arbitrary mode conversion between TE-polarized modes. Here, as examples, we present the performances of the two mode converters from $TE_0$ to $TE_1$ and from $TE_0$ to $TE_2$, which are based on tilted slot and bi-tilted slot respectively. The three-dimensional finite-difference time-domain (3D-FDTD) method is implemented to simulate the device performance.

The simulated electric field ($E_y$) distribution along the tilted slot and the bi-tilted slot at the wavelength of 1550 nm are shown in Fig. 4(a) and (b) respectively. For $TE_0$ converting to $TE_1$ in the tilted slot, it can be seen from Fig. 4(a) that the input $TE_0$ mode is firstly squeezed into a sharp corner on the BS1 and then scattered towards BS2. The propagating field is refocused into two beams of light with $\pi$ phase difference by BS2. Thus, $TE_0$ is converted into $TE_1$ completely. Likewise, in the bi-tilted slot, the mode conversion process based on multimode interference is shown in Fig. 4(b). However, due to the difference between the refractive index distributions in the bi-tilted slot and in the tilted slot, the propagating field is refocused into three beams of light by BS2 with $\pi$ phase difference. Therefore, $TE_0$ is converted into $TE_2$. Both the mode evolution process from $TE_0$ to $TE_1$ and from $TE_0$ to $TE_2$ agree well with the high-contrast index modulation introduced by tilted slot and bi-tilted slot. The parameters used in simulations are optimized and listed in Table 1.

Conversion efficiency and modal crosstalk are two important parameters to evaluate the performances of the mode converters. Conversion efficiency is defined as power ratio between the desired output mode and the input mode to evaluate the energy loss along the whole mode con-

TABLE 1
Optimized Parameters and Performances of the Mode Converter by 3D-FDTD Simulation at the Wavelength of 1550 nm

**at the wavelength of 1550 nm**

| Mode converter | $\alpha_1$ | $\alpha_2$ | $d_{slot}$ (μm) | $H_{etched.}$ (nm) | **Conversion efficiency** | **Modal crosstalk** |
|---|---|---|---|---|---|---|
| $TE_0$-to-$TE_1$ | 81.0° | 82.8° | 10.89 | 35.0 | 99.7% | -27.3 dB |
| $TE_0$-to-$TE_2$ | 77.0° | 81.5° | 0.86 | 75.0 | 99.4% | -26.4 dB |

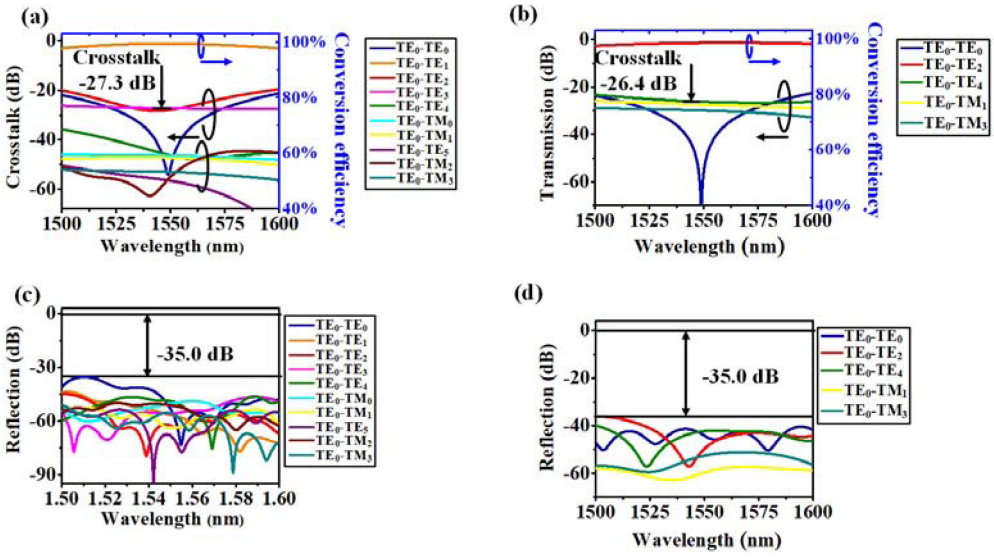


Fig. 5. Curves of modal crosstalk and conversion efficiency for (a) tilted slot (b) bi-tilted slot at the wavelength from 1500 nm to 1600 nm. Reflection spectra for (c)$TE_0$ converting to $TE_1$ and (d) $TE_0$ converting to $TE_2$.

verter. The modal crosstalk is defined to evaluate the mode purity and can be expressed as $max\{10log_{10}(P_i/P_d)\}$, where $P_i$ and $P_d$ are the transmitted power of the $i$th interfering modes and the desired mode, respectively [29].

The curves of modal crosstalk and conversion efficiency of the tilted slot are plotted in Fig. 5(a) from 1500 nm to 1600 nm. Modal crosstalk is lower than −20.0 dB with conversion efficiency higher than 97.6% over a 100 nm bandwidth, which indicates high mode purity and low loss. Meanwhile, we also simulated its reflection spectra as shown in Fig. 5(c). We found that reflections are all less than −35.0 dB from 1500 nm to 1600 nm. Therefore, the backscattering is highly suppressed, which is usually desired in the performances of photonic devices. The parameters used in the simulation and the optimized conversion efficiency and modal crosstalk are listed in Table 1.

In addition, curves of conversion efficiency, modal crosstalk and reflections are also simulated for bi-tilted slot and are plotted in the Fig. 5(b) and (d) respectively. High conversion efficiency (larger than 98%), low inter-modal crosstalk (lower than −23.0 dB) and low reflection (lower than −35.0 dB) are achieved from 1500 nm to 1600 nm over a 100 nm bandwidth. In addition, it is interesting to find that both in the transmission and reflection spectra in bi-tilted slot, the main modes are all odd modes which has same symmetry with the input mode. But for tilted slot, all the eigenmodes appears in the tilted slot. This phenomenon may be due to the symmetric index distribution introduced by the bi-tilted slot and will be further investigated in the discussion section.

High conversion efficiency and low modal crosstalk are achieved both in mode converter from $TE_0$ to $TE_1$ and from $TE_0$ to $TE_2$ with parameters optimized. According to the principle, there are three parameters that mainly affect the performances: (1) the angles of the two BSs of the slot $\alpha_1$

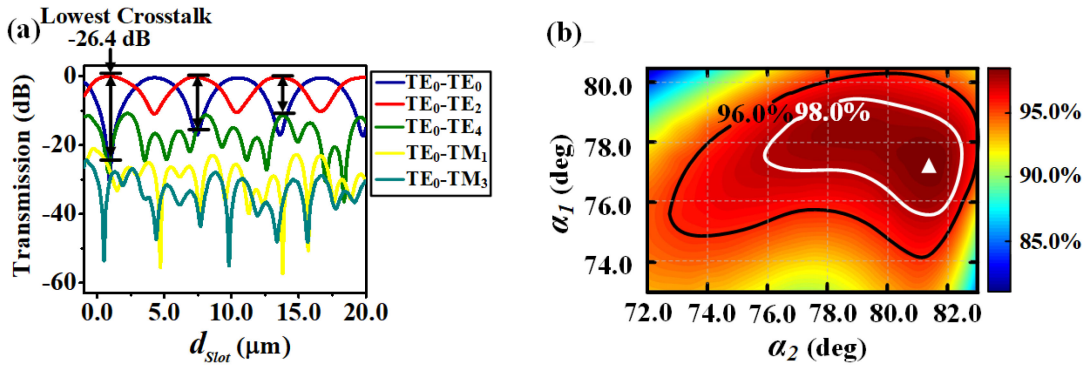


Fig. 6. For mode converter from $TE_0$ to $TE_2$, (a) simulated transmission spectra with the change of $d_{slot}$, and (b) simulated conversion efficiency under different $\alpha_1$ and $\alpha_2$. Here, for every set of $\alpha_1$ and $\alpha_2$, the $d_{slot}$ has been adjusted with highest conversion efficiency.

and $\alpha_2$; and (2) the distance between two BSs of the slot structure $d_{slot}$. Here, we take the mode converter from $TE_0$ to $TE_2$ as an example to analyze the influences on the optical performances.

At first, we investigate on influences of the distance between two BSs $d_{slot}$. We assume the angles of the two BSs of the slot $\alpha_1$ and $\alpha_2$ is already known ($\alpha_1 = 77.0°$ and $\alpha_2 = 81.5°$) and then simulate the performance of the bi-tilted slot with the change of $d_{slot}$. The simulated transmission responses are shown in Fig. 6(a). The parameters used in simulation are all listed in Table 1. Interestingly, with the increase of $d_{Slot}$, the conversion from $TE_0$ to $TE_2$ is periodic with the period of approximately 6.40 $\mu$m, which are in accordance with the self-imaging effect by multimode interference in the slot waveguide [27]. The effective refractive index of $TE_0^{Slot}$ and $TE_2^{Slot}$ are 2.46 and 2.22 in the slot waveguide, respectively. Therefore, their beat length is 3.16 $\mu$m according to $L_\pi = \pi/(\beta_{TE0} - \beta_{TE2})$, which is nearly a half of the period 6.40 $\mu$m. Fig. 6(a) shows that the optimal modal crosstalk of the mode converter is $-26.4$ dB when $d_{Slot}$ is 0.86 $\mu$m at the wavelength of 1550 nm. With further increase of $d_{Slot}$, the modal crosstalk would become worse due to the increased interaction with high order modes.

Secondly, we plot the distribution of the optimized conversion efficiency as a function of $\alpha_1$ and $\alpha_2$ at the wavelength of 1550 nm as shown in Fig. 6(b). Here, for each set of $\alpha_1$ and $\alpha_2$, the corresponding $d_{slot}$ is selected by obtaining the highest conversion efficiency as analyzed above. $\alpha_1$ and $\alpha_2$ can affect the high-contrast index distribution introduced by the two BSs and affect the multimode interference in the bi-tilted slot. It can be seen from Fig. 6(b) that the highest conversion efficiency that marked with a white triangle is 99.4% with the simulation parameters listed in Table 1. Besides, under a wide range of $\alpha_1$ (from 74.0° to 80.5°) and $\alpha_2$ (from 72.5° to 83.5°), a high conversion efficiency ($\geq$96.0%) can be obtained.

## 4. Fabrication Tolerance Analysis

The fabrication process of the proposed converter is simple. Only one-step lithography and etching process are required. However, because of the multimode interference in the polygonal slot, the device performance could be easily affected by the possible fabrication errors. Particularly, the sharp corners that appear in the slot structure is not easily realized in the fabrication. We can replace the sharp corners with round corners or use parabolic BSs in the real device fabrication. In this section, mode converter $TE_0$ to $TE_2$ is taken as an example to analyze the influences of the structure parameter variations such as the critical size of round corners $d_F$, the waveguide width $W_0$, the etched depth $H_{etched}$, and the angles of the two BSs $\alpha_1$ and $\alpha_2$.

As shown in Fig. 7(a), the round corners are designed to smoothly connect with the original BSs and it should be noted that when the $d_F$ is less than 150 nm, the proposed structure still remains good performance with conversion efficiency larger than 95% and modal crosstalk lower

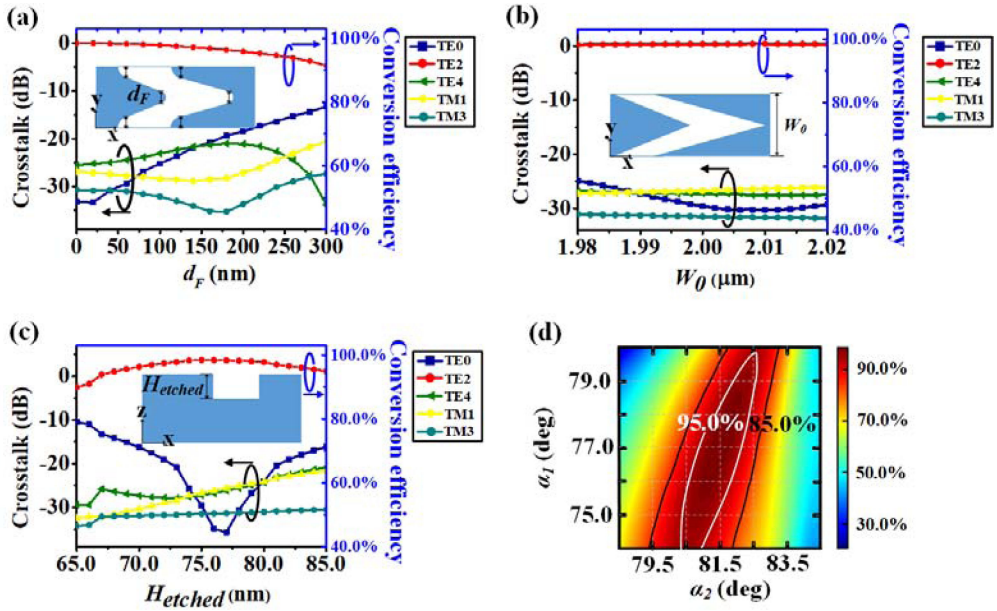


Fig. 7. For $TE_0$ converting to $TE_2$, simulated crosstalk and conversion efficiency with (a) round corner with critical size $d_F$ from 0 nm to 300 nm, (b) waveguide width errors within ±20.0 nm, (c) etched depth errors within ±10.0 nm, and (d) angle errors of $\alpha_1$ and $\alpha_2$.

than −20 dB. Even the $d_F$ is as large as 300 nm, the conversion efficiency is still larger than 90%, which shows high fabrication tolerance for round corners and can be realized with electron beam lithography (EBL) [30]. In addition, the performance of the mode converter from $TE_0$ to $TE_2$ almost remains unchanged with the variation of $W_0$ as shown in Fig. 7(b). When the variation of $W_0$ is as large as ±20.0 nm, the conversion efficiency larger than 98.0% and modal crosstalk less than −25.0 dB can be obtained.

Furthermore, we also simulated modal crosstalk and conversion efficiency of the proposed mode converter with the change of $H_{etched}$, which are shown in Fig. 7(c). It can be seen that the output $TE_0$ is sensitive to the $H_{etched}$. Nevertheless, conversion efficiency larger than 90.0% and modal crosstalk lower than −10.0 dB can still be ensured within an etching depth error of ±10.0 nm. In addition, fabrication variations of $\alpha_1$ and $\alpha_2$ are analyzed, which is shown in Fig. 7(d). When the deviations of $\alpha_1$ and $\alpha_2$ from −2.0° to +1.0° and from +3.0° to −3.0° respectively, the proposed mode converter can maintain high conversion efficiency (>85.0%). As a whole, the proposed structure based on polygonal slot shows good fabrication tolerance.

## 5. Discussion

Apart from the mode converter from $TE_0$ to $TE_1$ and from $TE_0$ to $TE_2$ that we analyzed above, based on the different polygonal slot, similar mode converters can also be designed. Here, to show the scalability of our TE-polarized mode converters, three examples are displayed in Fig. 8. Based on the even symmetry of the bi-tilted slot, mode conversion from $TE_1$ to $TE_3$ can also be realized and its mode evolution process with electric field ($E_y$) distribution is shown in Fig. 8(a). In addition, the tri-tilted slot can realize mode conversion from $TE_0$ to $TE_1$. However, the etched depth $H_{etched}$ that required for mode conversion is different. Fig. 8(b) displays the electric field ($E_y$) distribution at the wavelength of 1550 nm. The conversion efficiently is as high as 90% with the modal crosstalk is higher than −15 dB. Moreover, the total length is much shorter than tilted slot, which could be applied in systems that require ultra-compact sizes.

In addition, we can cascade the polygonal slots to realize more types of mode order conversions if the desired mode order conversion cannot be directly obtained by a single polygonal slot structure.

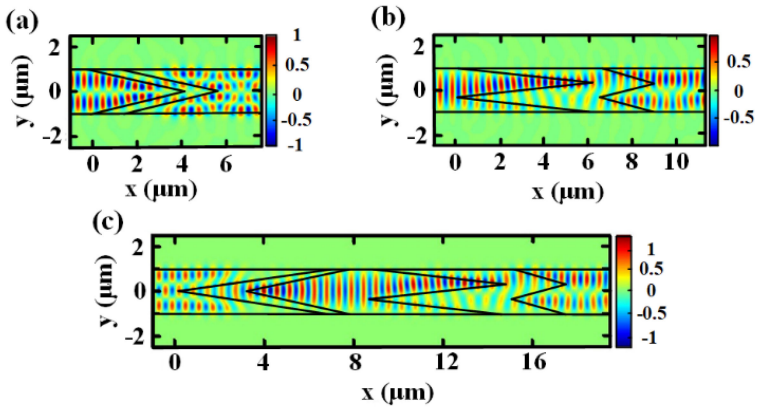


Fig. 8. Electric field ($E_y$) distribution along the mode converter (a) from $TE_1$ to $TE_3$ in the bi-tilted slot, (b) from $TE_0$ to $TE_1$ in the tri-tilted slot, (c) from $TE_2$ to $TE_1$ in the cascaded slots.

TABLE 2
Optimized Parameters of the Mode Converter in 3D-FDTD Simulation

| Mode converter | $\alpha_1$ | $\alpha_2$ | $d_{slot}$ (μm) | $H_{etched.}$ (nm) |
|---|---|---|---|---|
| $TE_1$-to-$TE_3$ | 75.0° | 75.0° | 1.40 | 120.0 |
| $TE_0$-to-$TE_1$ | 84.0° | 75.0° | 2.50 | 75.0 |
| $TE_2$-to-$TE_1$ | 81.5°(84°) | 77.0°(75.0°) | 0.86(2.5) | 75.0 |

Here, a mode converter from $TE_2$ to $TE_1$ is presented as an example for designing mode converters based on cascaded polygonal slots. The proposed structure is a bi-tilted slot followed by a tri-tilted slot. The optimized parameters for $TE_2$ converting to $TE_1$ at the wavelength of 1550 nm are all listed in Table 2. Fig. 8(c) shows the electric field ($E_y$) distribution in the proposed mode converter with optimized parameters.

## 6. Conclusion

In summary, we proposed a new type of mode converter based on deeply-etched polygonal slot in the silicon waveguide. With the high-contrast index modulation along the two BSs, multimode interference in the slot can be utilized for mode conversions. We proposed the mode converters from $TE_0$ to $TE_1$, $TE_0$ to $TE_2$, $TE_1$ to $TE_3$ based on tilted slot, bi-tilted slot and tri-tilted slot. In addition, by taking the mode converter from $TE_0$ to $TE_2$ as an example, we analyze the performances dependence on angles of the slot, the distance between two BSs of the slot and examine the fabrication tolerance for structure parameters. The proposed mode converter based on slot structure shows high conversion efficiency, low insertion loss, low modal crosstalk, broadband performance and good fabrication tolerance. Finally, we also discussed the cascaded slots to realize more mode conversions. Therefore, the proposed structure will be beneficial to the on-chip MDM systems with high-density integration in the future.

## References

[1] R. Nagarajan *et al.*, "Large-scale photonic integrated circuits," *IEEE J. Sel. Topic Quantum Electron.*, vol. 11, no. 1, pp. 50–65, Jan./Feb. 2005.
[2] J. Sun *et al.*, "Large-scale silicon photonic circuits for optical phased arrays," *IEEE J. Sel. Topic Quantum Electron.*, vol. 20, no. 4, pp. 264–278, Jul./Aug. 2014.
[3] P. T. Lin *et al.*, "Low-stress silicon nitride platform for mid-infrared broadband and monolithically integrated microphotonics," *Adv. Opt. Mater.*, vol. 1, no. 10, pp. 732–739, 2013.

[4] G. Chen, Y. Yu, and X. Zhang, "Monolithically mode division multiplexing photonic integrated circuit for large-capacity optical interconnection," *Opt. Lett.*, vol. 41, no. 15, pp. 3543–3546, 2016.
[5] L. Luo *et al.*, "WDM-compatible mode-division multiplexing on a silicon chip," *Nature Commun.*, vol. 5, 2014, Art. no. 3069.
[6] J. Wang, S. He, and D. Dai, "On-chip silicon 8-channel hybrid (de) multiplexer enabling simultaneous mode-and polarization-division-multiplexing," *Laser Photon. Rev.*, vol. 8, no. 2, pp. 18–22, 2014.
[7] K. T. Ahmmed, H. P. Chan, and B. Li, "Broadband high-order mode pass filter based on mode conversion," *Opt. Lett.*, vol. 42, no. 8, pp. 3686–3689, 2017.
[8] H. Xu and Y. Shi, "Ultra-broadband dual-mode 3 dB power splitter based on a Y-junction assisted with mode converters," *Opt. Lett.*, vol. 2, no. 6, pp. 5047–5050, 2016.
[9] B. Stern *et al.*, "On-chip mode-division multiplexing switch," *Optica*, vol. 41, no. 21, pp. 530–535, 2015.
[10] B. Desiatov, I. Goykhman, and U. Levy, "Nanoscale mode selector in silicon waveguide for on chip nanofocusing applications," *Nano Lett.*, vol. 9, no. 10, pp. 3381–3386, 2009.
[11] A. Fujie, S. Yuya, and M. Tetsuya, "Silicon waveguide optical isolator integrated with TE-TM mode converter," in *Proc. IEEE Opt. Fiber Commun. Conf. Exhib.*, 2015, pp. 1–3.
[12] P. Measor, S. Kühn, E. J. Lunt, B. S. Phillips, A. R. Hawkins, and H. Schmidt, "Multi-mode mitigation in an optofluidic chip for particle manipulation and sensing," *Opt. Exp.*, vol. 17, no. 26, pp. 24342–24348, 2009.
[13] R. Xiao *et al.*, "On-chip mode converter based on two cascaded Bragg gratings," *Opt. Exp.*, vol. 27, no. 3, pp. 1941–1957, 2019.
[14] D. Dai, Y. Tang, and J. E. Bowers, "Mode conversion in tapered submicron silicon ridge optical waveguides," *Opt. Exp.*, vol. 20, no. 12, pp. 13425–13439, 2012.
[15] J. B. Driscoll, R. R. Grote, B. Souhan, J. I. Dadap, M. Lu, and R. M. Osgood, "Asymmetric Y junctions in silicon waveguides for on-chip mode-division multiplexing," *Opt. Lett.*, vol. 38, no. 11, pp. 1854–1856, 2013.
[16] Y. Chaen, T. Ryota, and H. Kiichi, "Optical mode converter using multi-mode interference structure," in *Proc. IEEE Tech. Dig. 18th Microoptics Conf.*, 2013, pp. 1–2.
[17] D. Ohana and U. Levy, "Mode conversion based on dielectric metamaterial in silicon," *Opt. Exp.*, vol. 22, no. 22, pp. 27617–27631, 2014.
[18] H. Wang, Y. Zhang, Y. He, Q. Zhu, L. Sun, and Y. Su, "Compact silicon waveguide mode converter employing dielectric metasurface structure," *Adv. Opt. Mater.*, vol. 7, no. 4 2018, Art. no. 1801191.
[19] Z. Li *et al.*, "Controlling propagation and coupling of waveguide modes using phase-gradient metasurfaces," *Nature Nanotechnol.*, vol. 12, no. 7, pp. 675–683, 2017.
[20] L. H. Frandsen *et al.*, "Topology optimized mode conversion in a photonic crystal waveguide fabricated in silicon-on-insulator material," *Opt. Exp.*, vol. 22, no. 7, pp. 8525–8532, 2014.
[21] W. Ye, X. Yuan, Y. Gao, and J. Liu, "Design of broadband silicon-waveguide mode-order converter and polarization rotator with small footprints," *Opt. Exp.*, vol. 25, no. 26, pp. 33176–33183, 2017.
[22] R. Claps, V. Raghunathan, O. Boyraz, P. Koonath, D. Dimitropoulos, and B. Jalali, "Raman amplification and lasing inSiGe waveguides," *Opt. Exp.*, vol. 13, no. 7, pp. 2459–2466, 2005.
[23] L. Ulf, "Optical conformal mapping," *Science*, vol. 312, no. 23, pp. 1777–1780, 2006.
[24] J. B. Pendry, D. Schurig, and D. R. Smith, "Controlling electromagnetic fields," *Science*, vol. 312, no. 23, pp. 780–1782, 2006.
[25] Y. G. Ma, N. Wang, and C. K. Ong, "Application of inverse, strict conformal transformation to design waveguide devices," *J. Opt. Soc. America A*, vol. 27, no. 5, pp. 968–972, 2010.
[26] T. A. Driscoll, "Algorithm 843: improvements to the Schwarz-Christoffel toolbox for MATLAB," *ACM Trans. Math. Softw.*, vol. 31, no. 2, pp. 239–251, 2005.
[27] T. Ma, A. B. Khanikaev, S. H. Mousavi, and G. Shvets, "Guiding electromagnetic waves around sharp corners: Topologically protected photonic transport in metawaveguides," *Phys. Rev. Lett.*, vol. 114, no. 12, 2015, Art. no. 127401.
[28] M. Bachmann, Maurus, P. A. Besse, and H. Melchior, "General self-imaging properties in N× N multimode interference couplers including phase relations," *Appl. Opt.*, vol. 33, no. 18, pp. 3905–3911, 1994.
[29] H. Xu and Y. Shi, "Ultra-broadband dual-mode 3 dB power splitter based on a Y-junction assisted with mode converters," *Opt. Lett.*, vol. 41, no. 12, pp. 5047–5050, 2016.
[30] C. Vieu *et al.*, "Electron beam lithography: Resolution limits and applications." *Appl. Surf. Sci.*, vol. 164, pp. 111–117, 2000.